

Electronic Supplementary Information

Phase transition from hexagonal LnF_3 ($\text{Ln}=\text{La, Ce, Pr}$) to cubic $\text{Ln}_{0.8}\text{M}_{0.2}\text{F}_{2.8}$ ($\text{M}=\text{Ca, Sr, Ba}$) nanocrystals with enhanced upconversion induced by alkaline-earth doping

Daqin Chen ^a, Yunlong Yu ^a, Feng Huang ^a, and Yuansheng Wang ^{*a,b}

^aState Key Laboratory of Structural Chemistry, Fujian Institute of Research on the Structure of Matter, Chinese Academy of Sciences, Fuzhou, China

^bState Key Laboratory of Optoelectronic Materials and Technologies, Sun Yat-sen University, Guangzhou, China

*Address correspondence to E-mail: yswang@fjirsm.ac.cn

Experimental details

Materials. All the chemicals were of analytical grade and used as received without further purification. Deionized water was used throughout. $\text{M}(\text{NO}_3)_2$ ($\text{M}=\text{Ca}^{2+}$, Sr^{2+} , Ba^{2+}), $\text{Ln}(\text{NO}_3)_3 \cdot 6\text{H}_2\text{O}$ ($\text{Ln}=\text{La}^{3+}$, Ce^{3+} , Pr^{3+} , Tb^{3+} , Eu^{3+} , Er^{3+} , Tm^{3+} , Yb^{3+}), oleic acid, sodium oleate (NaOA), ethanol and HF (40wt %) were all supplied by Sinopharm Chemical Reagent Company.

Synthesis of nanoparticles. The M^{2+} doped LnF_3 NCs were prepared by a modified liquid-solid-solution (LSS) solvothermal route firstly reported by Li et al.¹⁸⁻²² In a typical synthesis of LnF_3 nanoparticles, an aqueous solution of cerium salt (0.5 mol/L) was mixed with ethanol (20 mL), oleic acid (20 mL) and NaOA (5.0 g) under thorough stirring. Then, 4mL HF (1.0 mol/L) solution was dropwise added to the mixture. After vigorous stirring at room temperature for 30 min, the colloidal solution were transferred into a 100 mL Teflon-lined autoclave, sealed and heated at 130 °C for 12 h. The final products were collected, washed for several times with ethanol/cyclohexane, and purified by centrifugation. The introduction of alkaline-earth ions (such as Ca^{2+} , Sr^{2+} , Ba^{2+}) and/or rare earth ions (such as Eu^{3+} , $\text{Yb}^{3+}/\text{Er}^{3+}$, $\text{Yb}^{3+}/\text{Tm}^{3+}$) was achieved by adding the corresponding metal salts with designed concentrations.

Characterizations. XRD analysis was carried out with a powder diffractometer (DMAX2500 RIGAKU) using $\text{CuK}\alpha$ radiation ($\lambda=0.154$ nm). The size, shape and phase structure of the samples were studied by a transmission electron microscope

(TEM, JEM-2010) equipped with an energy dispersive x-ray spectroscope (EDS). TEM specimens were prepared by directly drying a drop of a dilute cyclohexane dispersion solution of the products on the surface of a carbon-coated copper grid. The valence states and the actual composition of the products were detected by X-ray photoelectron spectroscopy (XPS) using a VG Scientific ESCA Lab Mark II spectrometer equipped with two ultra-high vacuum 6 (UHV) chambers. All the binding energies were referenced to the C_{1s} peak of the surface adventitious carbon at 284.8 eV. The photoluminescence, photoluminescence excitation spectra and decay curves (time-resolved luminescence spectra) were recorded by an Edinburgh Instruments FLS920 spectrofluorometer equipped with both continuous (450 W) and pulsed xenon lamps. The upconversion emission spectra were detected using the Hamamatsu R943-02 PMT and a Spex 1000M monochromator under a power-adjustable laser diode (975 nm) excitation. To enable comparison of the upconversion emission intensities among different samples, the emission spectra were measured with the same instrumental parameters (for example: same excitation wavelength and power, same excitation and emission slits). All the measurements were carried out at room temperature.

Figure S1-S14:

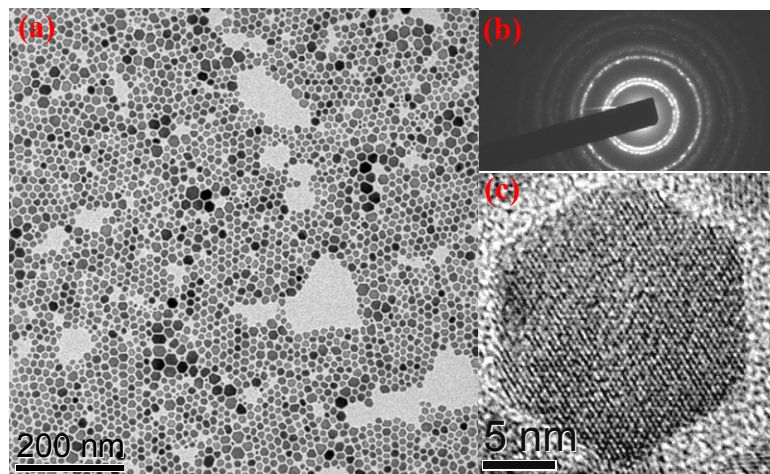


Figure S1. (a) TEM micrograph of 5 mol% Ca^{2+} doped CeF_3 sample, (b) the corresponding SAED pattern, and (c) HRTEM image of an individual nanocrystal.

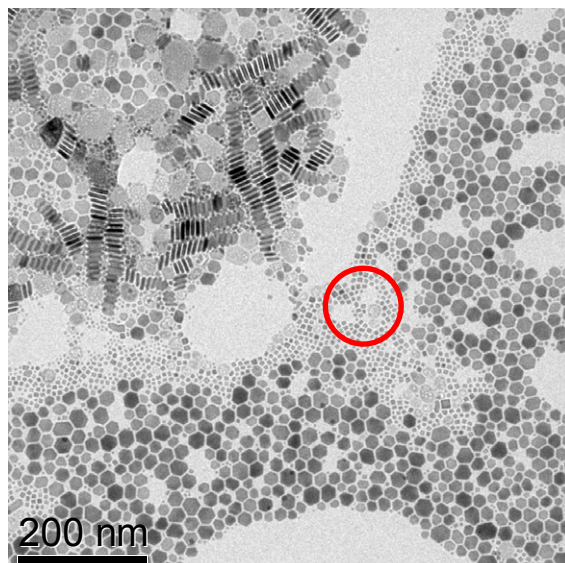


Figure S2. TEM micrograph of 10 mol% Ca^{2+} doped CeF_3 sample

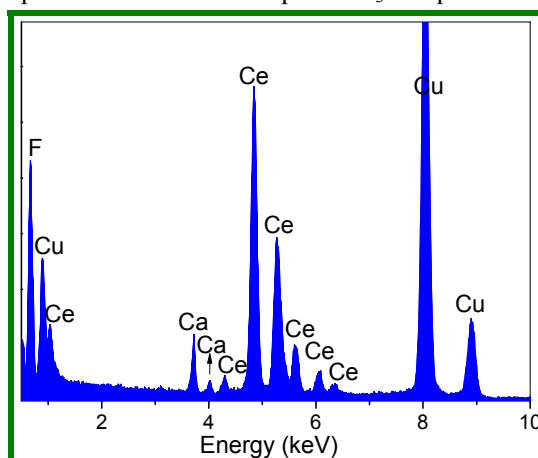


Figure S3. EDS spectrum taken from the 20 mol% Ca^{2+} doped CeF_3 sample (Cu signals come from the copper grid)

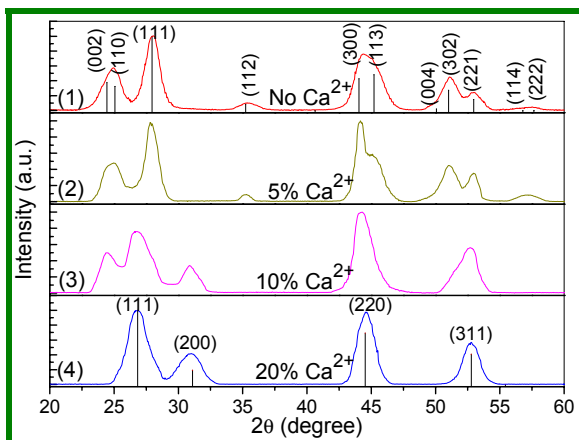


Figure S4. XRD patterns of (1) pure, (2) 5 mol%, (3) 10 mol%, and (4) 20 mol% Ca^{2+} doped CeF_3 samples; the bars in (1) and (4) represent the standard hexagonal CeF_3 and cubic CeF_2 crystalline data, respectively.

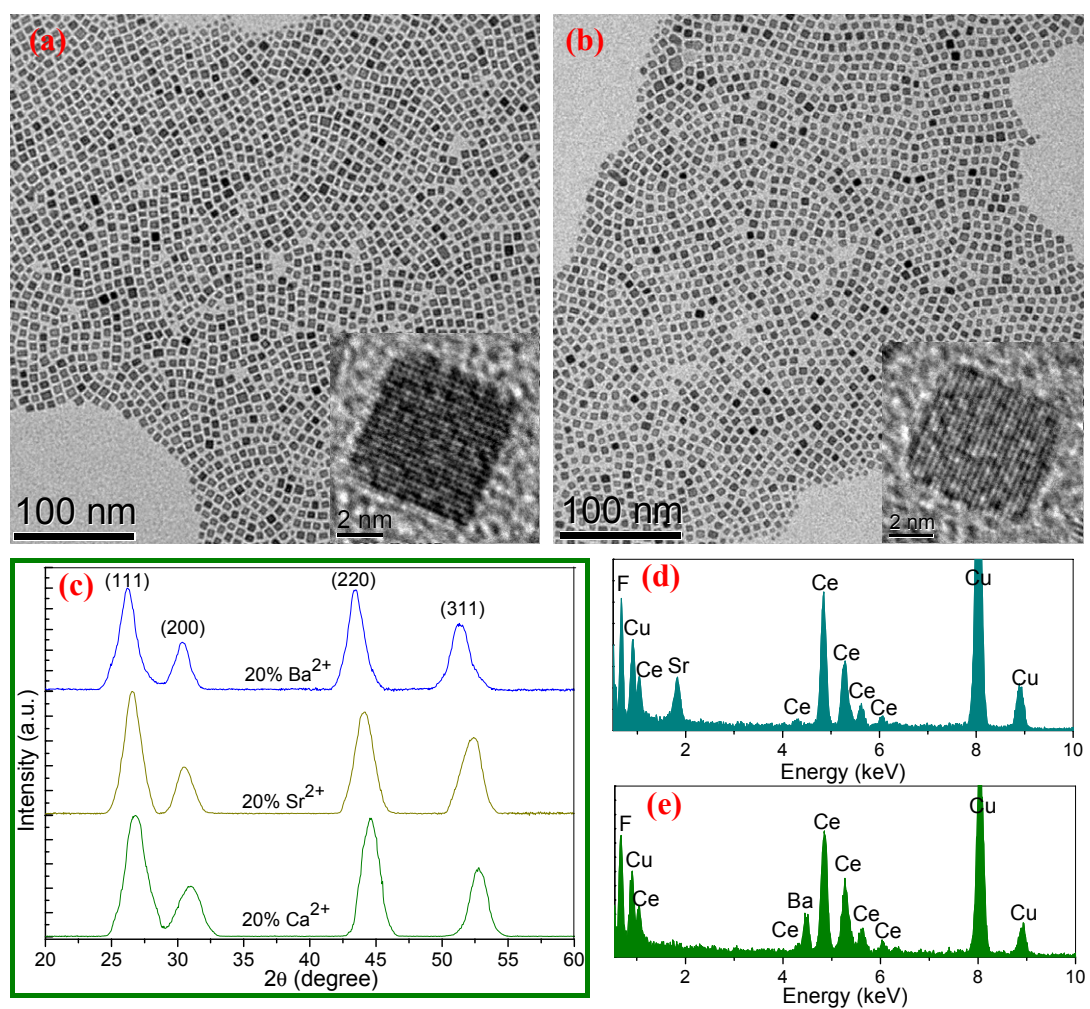


Figure S5. TEM micrographs of (a) 20 mol% Sr^{2+} , and (b) 20 mol% Ba^{2+} doped CeF_3 samples; insets shows HRTEM images of the individual nanocrystal in (a) and (b); (c) XRD patterns of 20 mol% M^{2+} ($\text{M}^{2+}=\text{Ca}^{2+}, \text{Sr}^{2+}, \text{Ba}^{2+}$) doped CeF_3 samples; (d-e) EDS spectra taken from nanocrystals in (a) and (b) respectively (Cu signals come from the copper grid).

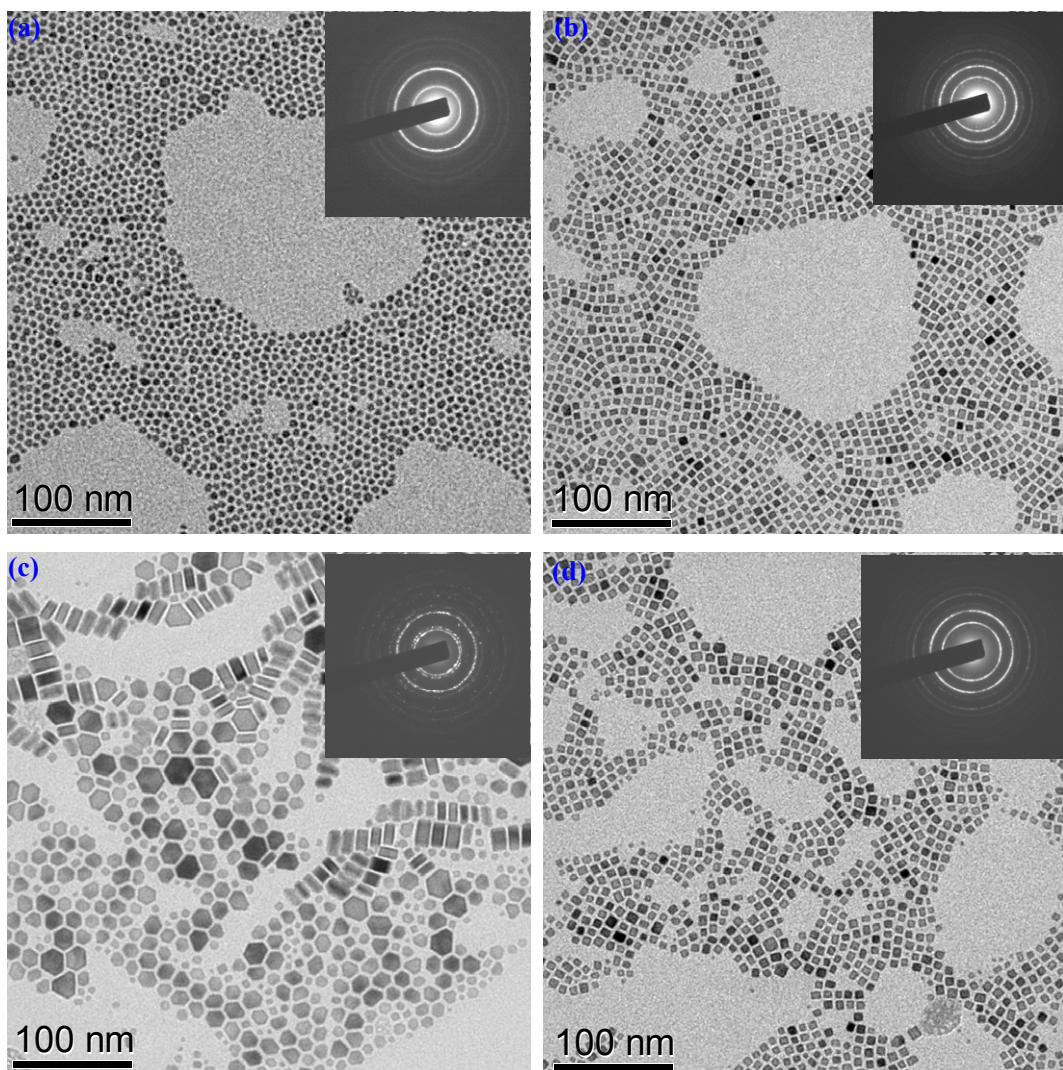


Figure S6. TEM micrographs of (a) pure, and (b) 20 mol% Ca²⁺ doped LaF₃ samples; TEM micrographs of (c) pure, and (d) 20 mol% Sr²⁺ doped PrF₃ samples; insets show the corresponding SAED patterns.

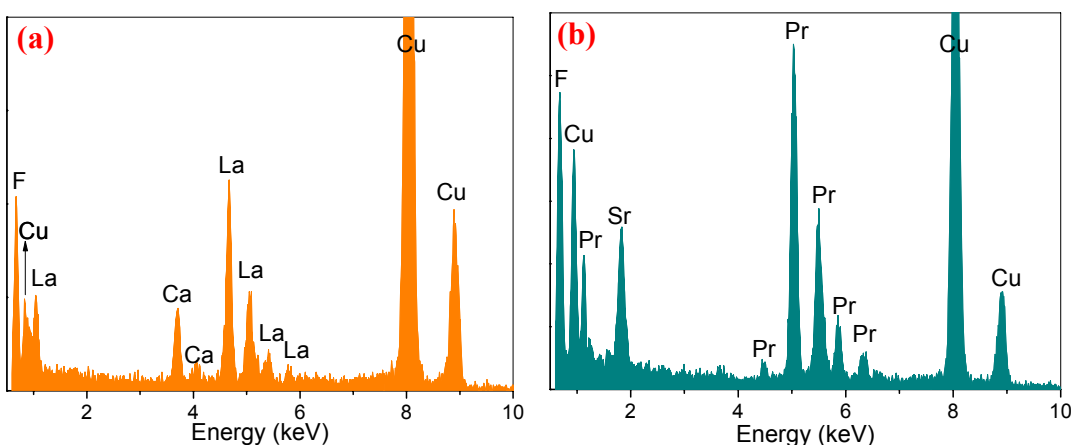


Figure S7. EDS spectra taken from (a) 20 mol% Ca²⁺ doped LaF₃, and (b) 20 mol% Sr²⁺ doped PrF₃ (Cu signals come from the copper grid).

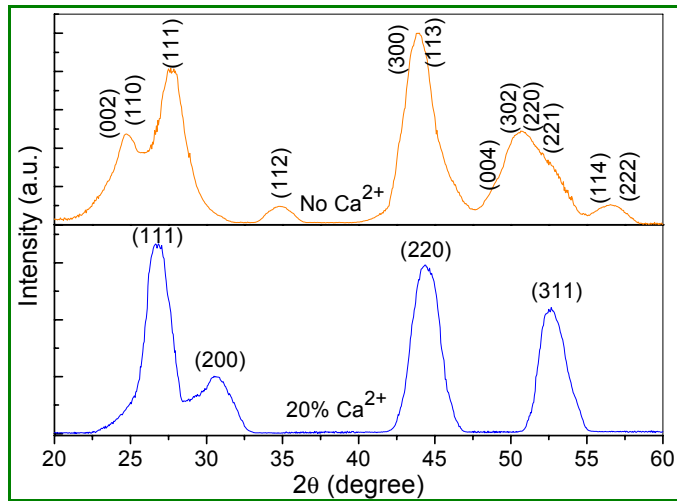


Figure S8. XRD patterns of pure and 20 mol% Ca^{2+} doped LaF_3 samples.

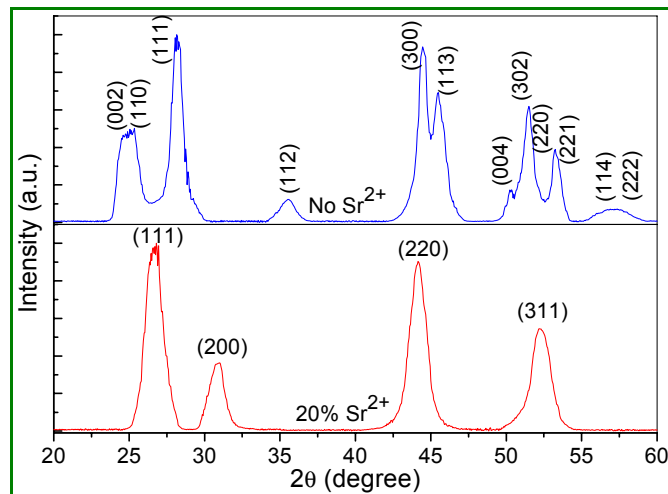


Figure S9. XRD patterns of pure and 20 mol% Sr^{2+} doped PrF_3 samples.

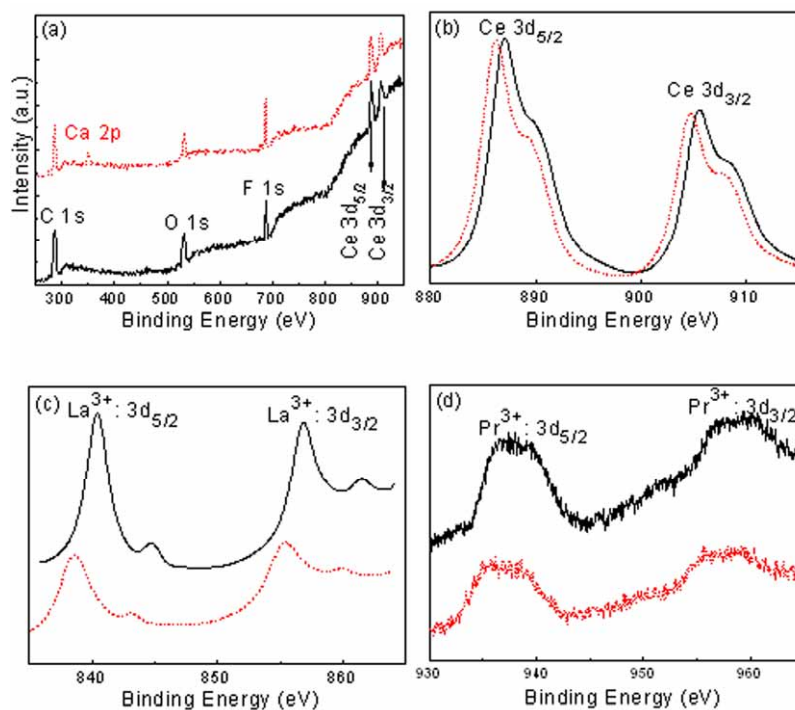


Figure S10. XPS full spectra taken from (a) un-doped (solid line), and 20 mol% Ca²⁺ doped (dotted line) CeF₃ samples; (b), (c) and (d) are slow-scanning XPS spectra of undoped (solid line) and 20 mol% Ca²⁺ doped (dotted line) CeF₃, LaF₃ and PrF₃ samples, respectively.

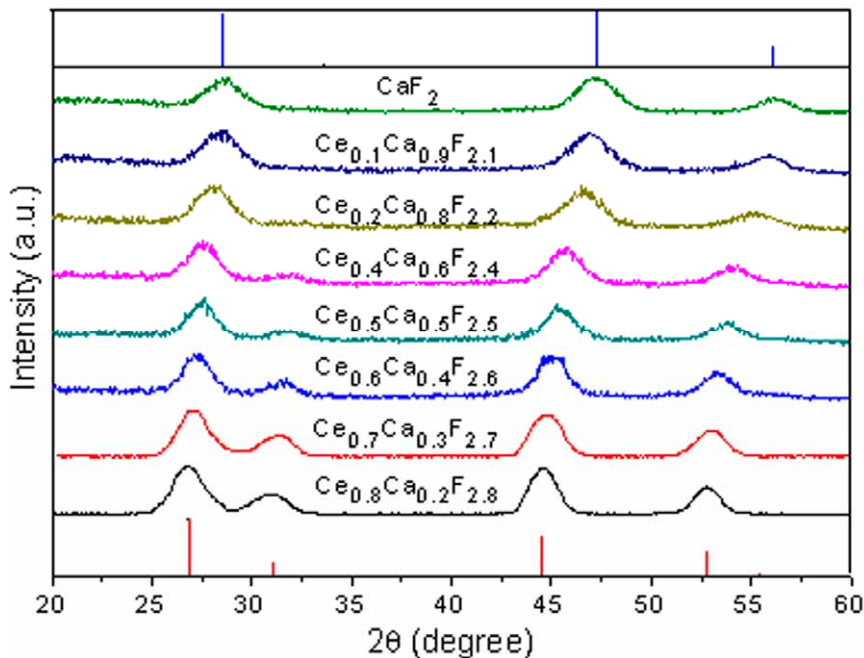


Figure S11. XRD patterns of Ce_{1-x}Ca_xF_{3-x} ($x=0.2, 0.3, 0.4, 0.5, 0.6, 0.8, 0.9, 1.0$) solid solutions; the bars in bottom and top represent the standard cubic CeF₂ and CaF₂ crystalline data, respectively.

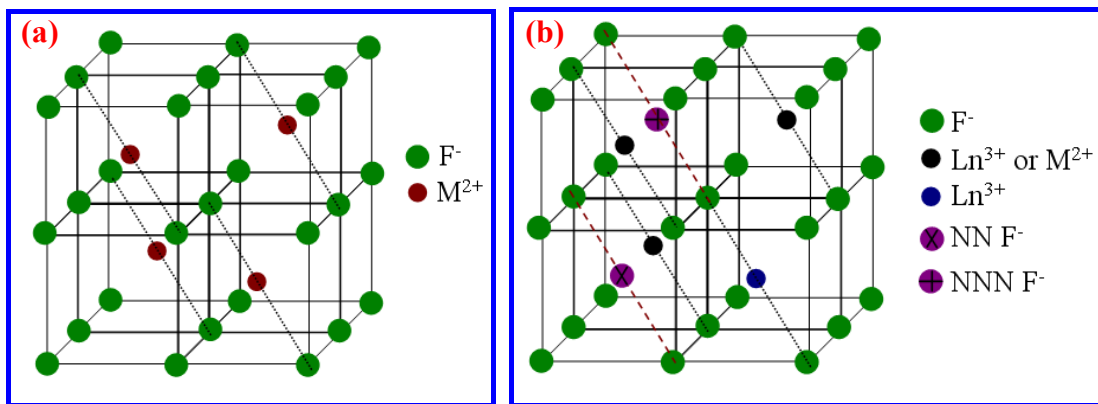


Figure S12. Schematic presentation of cubic structured MF_2 (a), and $\text{Ln}_{0.8}\text{M}_{0.2}\text{F}_{2.8}$ (b) phases; the local charge compensation for each Ln^{3+} ion in $\text{Ln}_{0.8}\text{M}_{0.2}\text{F}_{2.8}$ is achieved by the occupation of a F^- ion in the nearest-neighbor (NN) or next-nearest-neighbor (NNN) site with respect to the Ln^{3+} ion.

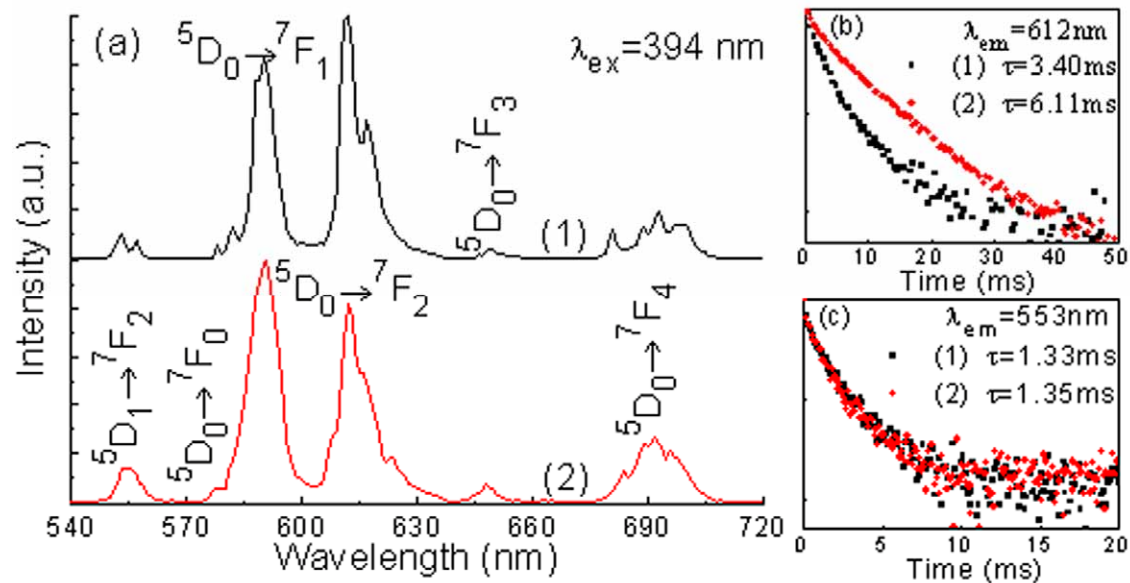


Figure S13. Emission spectra of (a) $\text{La}_{0.95}\text{Eu}_{0.05}\text{F}_3$ (1), and $\text{La}_{0.75}\text{Eu}_{0.05}\text{Sr}_{0.2}\text{F}_{2.8}$ (2) NCs; (b) and (c) are decay curves of Eu^{3+} : $^5\text{D}_0$ and Eu^{3+} : $^5\text{D}_1$ levels.

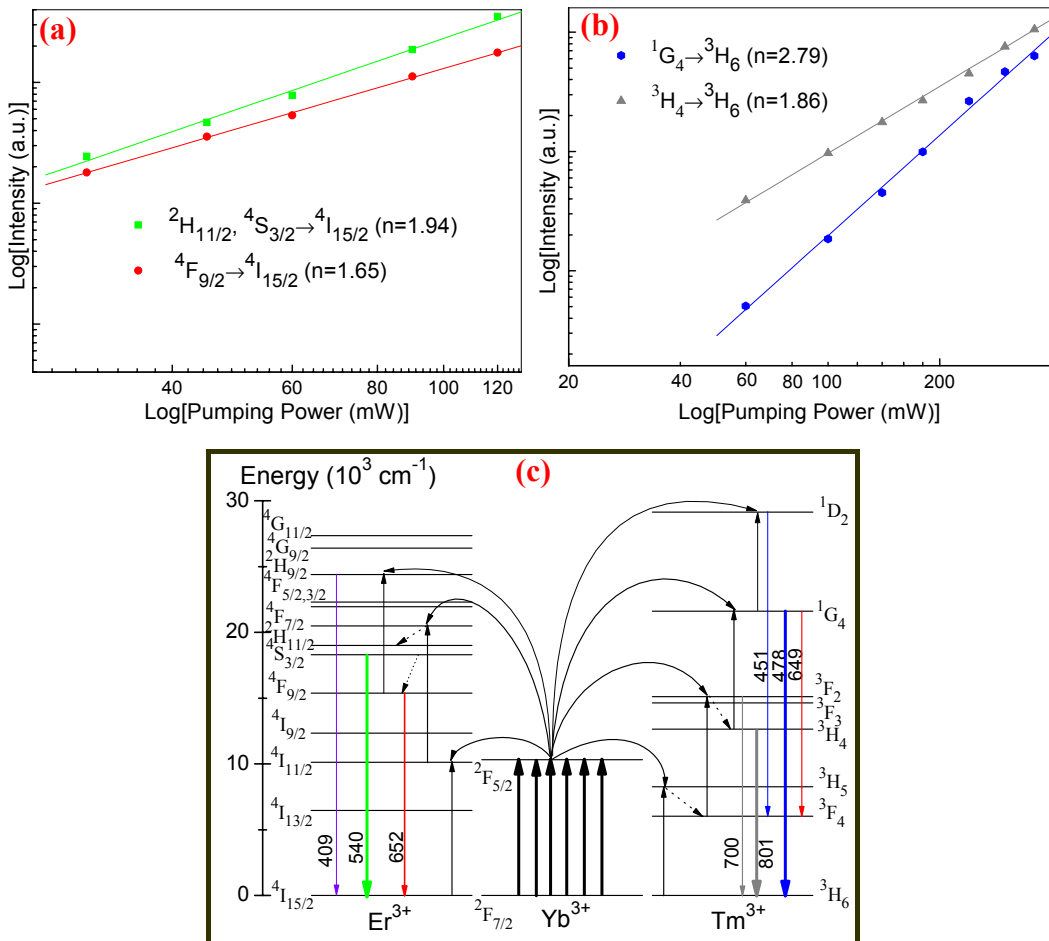


Figure S14. Log-log plot of upconversion emission intensity versus excitation power of (a) $\text{La}_{0.69}\text{Yb}_{0.1}\text{Er}_{0.01}\text{Sr}_{0.2}\text{F}_{2.8}$, and (b) $\text{La}_{0.69}\text{Yb}_{0.1}\text{Tm}_{0.01}\text{Sr}_{0.2}\text{F}_{2.8}$ nanocubes dissolved in cyclohexane, showing that two and three pumping photons are required to populate the $\text{Er}^{3+}:^2\text{H}_{11/2}$, $^4\text{S}_{3/2}$ and $\text{Tm}^{3+}:^1\text{G}_4$ emitting levels respectively; (c) energy level diagram of Er^{3+} , Tm^{3+} and Yb^{3+} ions, showing the possible upconversion mechanisms of the samples.